**Annales
Geophysicae**

Magnetospheric response to the solar wind as indicated by the cross-polar potential drop and the low-latitude asymmetric disturbance field

S. Eriksson, L. G. Blomberg, N. Ivchenko, T. Karlsson, and G. T. Marklund

Alfvén Laboratory, Royal Institute of Technology, SE-10044 Stockholm, Sweden

Abstract. The cross-polar potential drop Φ_{pc} and the low-latitude asymmetric geomagnetic disturbance field, as indicated by the mid-latitude *ASY-H* magnetic index, are used to study the average magnetospheric response to the solar wind forcing for southward interplanetary magnetic field conditions. The state of the solar wind is monitored by the ACE spacecraft and the ionospheric convection is measured by the double probe electric field instrument on the Astrid-2 satellite. The solar wind-magnetosphere coupling is examined for 77 cases in February and from mid-May to mid-June 1999 by using the interplanetary magnetic field B_z component and the reconnection electric field. Our results show that the maximum correlation between Φ_{pc} and the reconnection electric field is obtained approximately 25 min after the solar wind has reached a distance of 11 R_E from the Earth, which is the assumed average position of the magnetopause. The corresponding correlation for *ASY-H* shows two separate responses to the reconnection electric field, delayed by about 35 and 65 min, respectively. We suggest that the combination of the occurrence of a large magnetic storm on 18 February 1999 and the enhanced level of geomagnetic activity which peaks at $Kp = 7^-$ may explain the fast direct response of *ASY-H* to the solar wind at 35 min, as well as the lack of any clear secondary responses of Φ_{pc} to the driving solar wind at time delays longer than 25 min.

Key words. Magnetospheric physics (solar wind-magnetosphere interactions; plasma convection) – Ionosphere (electric fields and currents)

1 Introduction

The study of high-latitude ionospheric convection and its response to changes in the solar wind is important for the understanding of the dynamic solar wind-magnetosphere coupling process. Several studies of the large-scale convection electric field have shown that it generally takes 10–20 min

Correspondence to: S. Eriksson (eriksson@plasma.kth.se)

for the global polar cap convection to adjust itself following a southward turning of the interplanetary magnetic field (IMF) at the dayside magnetopause (Holzer and Reid, 1975; Etemadi et al., 1988; Todd et al., 1988; Eriksson et al., 2000). This time scale was also found in studies correlating the geomagnetic *AL* index with the solar wind motional electric field vB_s (Iyemori et al., 1979; Bargatze et al., 1985; Blanchard and McPherron, 1995), where v is the solar wind velocity, and $B_s = -B_z$ for southward IMF and is, otherwise, zero. A second characteristic time scale with approximately a 60 min delay emerged from these studies as well, which was suggested as the delayed unloading response of the geomagnetic tail. The initial 10–20 min time scale is explained as the delay introduced by having a finite Pedersen conductivity in the polar cap and auroral oval regions (Sanchez et al., 1991). Clauer et al. (1983) also investigated the coupling between the solar wind electric field and the horizontal component of the low-latitude asymmetric geomagnetic disturbance field, which resulted in a peak response of the asymmetric disturbance delayed by approximately 60 min.

The disturbance in the low-latitude geomagnetic field consists of two parts. The first is a negative depression which is uniform in magnetic longitude and associated with the symmetric ring current. The second is a longitude-dependent asymmetric component that displays a stronger negative disturbance during evening hours than in the morning region, as observed with a longitudinal chain of ground magnetometers (Clauer and McPherron, 1980, and references therein).

Fukushima and Kamide (1973) and Crooker and Siscoe (1981) found that the greatest contribution to this dawn-dusk asymmetry in the horizontal geomagnetic field comes from field-aligned currents. Whether these field-aligned currents are part of a dusk centered partial ring current, closing in the ionosphere, or the result from an incomplete cancellation of the region 1 and region 2 current systems at noon and at midnight (Harel et al., 1981; Crooker and Siscoe, 1981) is still an open question.

Iyemori and Rao (1996) quantified the low-latitude asymmetric disturbance in the horizontal direction by the *ASY-H*
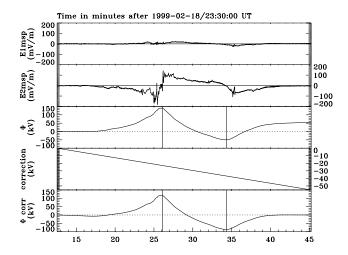
Fig. 1. First three panels show the two measured components of the electric field in the spin plane and the calculated potential along this dawn-to-dusk orbit above 40° corrected geomagnetic latitude. The last two panels show the potential correction assuming a return to zero potential at low latitudes and the resulting corrected potential. The corotation electric field has been subtracted.

index, which reportedly is essentially the same as the asymmetric indices proposed by Clauer and McPherron (1980) and Clauer et al. (1983).

In this paper, we will examine the separate statistical responses of polar cap convection and the field-aligned current system, which is believed to cause the low-latitude disturbance to the solar wind. The large-scale convection and the geomagnetic disturbance are measured by the cross-polar potential drop, Φ_{pc}, and the *ASY-H* index, respectively.

2 Data

The Swedish Astrid-2 micro-satellite was launched on 10 December 1998 into an 83° inclination polar orbit at 1000 km altitude and was spin-stabilized with a roughly Sun-pointing spin axis. In February and from mid-May until mid-June 1999, the satellite trajectory was in the dawn-dusk meridian plane and the probability of measuring most of the cross-polar potential drop Φ_{pc} was then at its peak. An initial set of 101 two-cell convection events was singled out in the northern hemisphere throughout this period, assuming a symmetric noon-midnight two-cell convection pattern.

This assumption is incorrect, however. The interplanetary magnetic field (IMF) has a clear influence on the distribution of electric potential in the polar cap region. As the IMF B_y goes from negative to positive for a given southward IMF, the location of the two potential extrema in the northern hemisphere rotates clockwise in magnetic local time (e.g. Shue and Weimer, 1994). Using the time shifted IMF and solar wind bulk velocity from the ACE spacecraft as input to the ionospheric convection model developed by Weimer (1996), we can produce a statistical convection pattern at the time of each Astrid-2 polar cap pass. The selection of events is

then optimized to where the satellite passes either through, or close to, both extrema of the Weimer model two-cell convection pattern. We further limit the data set to events where the IMF $B_z < 2$ nT 15 min prior to each polar cap pass to ensure the existence of a simple two-cell convection pattern.

Figure 1 shows the electric field along the orbit of one of the 77 polar cap passes that remained after applying these criteria. The first two panels show the two components of the measured electric field in a model magnetic field B and spin plane coordinate system. The third component, $E3_{msp}$, along the Sun-pointing spin axis is not measured. $E2_{msp}$ is in the spin plane, perpendicular to B and points in the dawn to dusk direction. $E1_{msp}$ completes the system. The corotation electric field and the induced $v \times B$ electric field due to the motion of the satellite through the Earth's magnetic field have both been subtracted from the measured field.

The electric potential Φ along the satellite trajectory is calculated by integrating the electric field above 40° corrected geomagnetic latitude (CGLat) for all passes, assuming that the spin axis electric field is zero. An example of the resulting electric potential is shown in panel three of Fig. 1. Theoretically, Φ should return to zero potential at low latitudes due to the shielding effect of the plasmasphere (Shue and Weimer, 1994). The reason why there is usually a mismatch may be due to several contributing sources of error. First, we employ a model magnetic field instead of the measured field. Second, even though we find it reasonable to approximate the missing axial component of the electric field to be zero, due to the orientation of the orbital plane and the spin plane, it is, indeed, unknown. Finally, the measurement accuracy of the electric field on Astrid-2 is estimated to be approximately 3 to 5 mV/m. By adding a constant electric field of 3.8 mV/m, corresponding to the electric potential offset that is observed for the case shown in Fig. 1, we correct for the total effect of these errors and force the low latitude potential back to zero (see the last two panels in Fig. 1).

The potential drop Φ_{pc} is essentially a time averaged quantity, since it is acquired over the time in between the two large-scale convection reversals (marked by vertical bars in Fig. 1). We, therefore, average the 1-min resolution *ASY-H* index over the same time interval, which is identified by its middle time, t_m, so that both quantities are comparable in time.

The time it takes for the solar wind to propagate from the ACE spacecraft, at the $L1$-point, to an average magnetopause location of 11 R_E (Fairfield, 1971), is computed individually for each measurement of Φ_{pc} by taking the mean of the solar wind bulk velocity two hours prior to t_m, and applying both the x_{gse} and y_{gse} velocity components (Eriksson et al., 2000). As a consequence of the finite Pedersen conductivity in the high-latitude ionosphere, we expect the large-scale convection electric field to gradually respond after some additional time delay following the arrival of a solar wind structure at the magnetopause (e.g. Sanchez et al., 1991). The time of zero magnetospheric time lag is defined here by subtracting only the propagation time from t_m for each event.
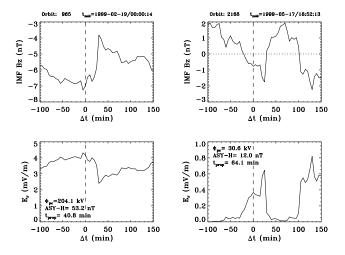
In order to estimate the average time delayed response for

Fig. 2. The time shifted IMF B_z and reconnection electric field E_r measured at the ACE spacecraft are plotted versus time lag Δt. A negative time lag refers to future solar wind conditions. Note the different vertical ranges on the y-axes.
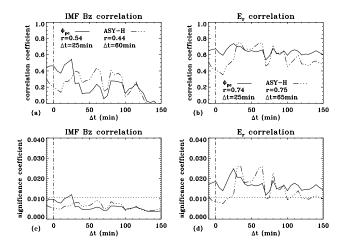

Fig. 3. Solar wind-magnetosphere correlation with **(a)** IMF B_z, and **(b)** reconnection electric field. The corresponding filtered correlation coefficients are shown in **(c)** and **(d)**, where the horizontal line marks $r = 0.50$. Time resolution is 5 min. The maximum correlation coefficients and corresponding time lag Δt are shown on each panel.

the two sets of Φ_{pc} and *ASY-H* to the driving solar wind, we will study how their correlation coefficients with two solar wind quantities evolve as a function of time lag.

3 Magnetospheric response to the solar wind

The applied solar wind quantities, both in GSM coordinates, are the IMF B_z and the model reconnection electric field $E_r = vB_t \sin^4(\theta/2)$, respectively. Here, v is the solar wind bulk velocity in x_{gsm} direction, B_t is the projection of the IMF onto the GSM $y - z$ plane, and θ is the clock angle between B_t and the positive z_{gsm} direction. These solar wind parameters have been shown to correlate well with the cross-polar potential drop (Reiff and Luhmann, 1986; Eriksson et al., 2000, and references therein).

Figure 2 shows the time shifted IMF B_z and E_r versus time lag Δt for two cases plotted next to each other. The measured potential drop along the orbit and the average *ASY-H* are indicated explicitly for both events, as well as the propagation time and the mid-time t_m. We observe that the potential drop and the low-latitude asymmetric geomagnetic disturbance are, indeed, larger for a correspondingly larger IMF B_z and electric field, as expected.

We now proceed to calculate a correlation coefficient between the set of 77 cross-polar potential drops and the two corresponding sets of solar wind parameters at $\Delta t=0$. For each new 5-min resolution time lag in the range -10 to 150 min, we calculate a new correlation coefficient as the solar wind parameters are changed (see Fig. 2 for the solar wind input as a function of time lag for two of the 77 events). The resulting correlation coefficients for both Φ_{pc} and *ASY-H* with the solar wind as a function of time lag is illustrated in Fig. 3a-b. The maximum correlation coefficient r and its corresponding time lag Δt are shown for each combination of magnetospheric parameter and solar wind quantity.

Since we are more interested in correlation coefficients above $r = 0.50$ than below, we filter the correlation coefficients through $y(r) = a \tan(r + c)$, where $a = 1/200.071$ and $c = 0.6349$ are two constants found by a minimum least squares functional fit of the data in Eriksson et al. (2000). The filter is based on a bootstrap technique (Efron and Tibshirani, 1993) for the derivation of a correlation coefficient standard error, which is used to quantify the bootstrap distribution produced for each correlation coefficient. This filter was recently developed by Eriksson et al. (2000). The resulting non-normalized filtered correlation coefficients y, here referred to as significance coefficients, are shown in Fig. 3c-d. The lower horizontal dotted line marks the level of $r = 0.50$. We see that the Φ_{pc} response to the reconnection electric field peaks at $\Delta t = 25$ min after which it slowly decays, whereas *ASY-H* first responds after about 35 min, then at 65 min, and finally shows an increased response at $\Delta t = 80$ min. The first two peaks have a correlation coefficient $r = 0.75$, while the last peak has $r = 0.72$.

4 Results and discussion

It has been shown in previous studies that Φ_{pc} generally correlates better with parameters including both the solar wind velocity and the IMF B_z, than with IMF B_z alone (e.g. Baker et al., 1983; Reiff and Luhmann, 1986; Eriksson et al., 2000). This is again evident in comparing the correlation coefficients for IMF B_z and E_r with Φ_{pc} in Fig. 3a-b.

The data and time lags for which the correlation is maximized between Φ_{pc} and the two solar wind quantities are shown in Fig. 4a-b along with an expression for its best linear fit (solid line). The corresponding linear fits (dashed line) from a recent study using the FAST satellite and the Wind
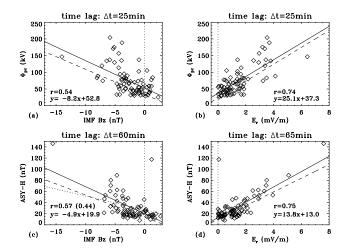
Fig. 4. Cross-polar potential drop versus **(a)** IMF B_z, and **(b)** E_r at the time lag of peak correlation. *ASY-H* versus **(c)** IMF B_z and **(d)** E_r, also for optimum time lag. Best linear fit for Astrid-2 and ACE spacecraft (solid line), and for FAST and Wind spacecraft (dashed line).

spacecraft (Eriksson et al., 2000) that comprised 37 events, are shown as well, and we see that the slopes are in good agreement. The optimized time lags for Φ_{pc} in the FAST study were found to be 15 min for both IMF B_z and E_r. This response peak was interpreted as the direct or driven magnetospheric response to the solar wind input and confirmed the line-tying time scale previously reported (Lockwood et al., 1990; Sanchez et al., 1991). The Φ_{pc} response to E_r was followed by two minor peaks at time lags Δt=55 min and Δt=105 min. These secondary pulses were both interpreted as unloading responses of the magnetotail.

Here, the maximum response for Φ_{pc} is approximately 25 min. The difference in time lag between the two studies is most likely due to the different positions of the two solar wind upstream monitors. Wind was located closer than 90 R_E upstream of the Earth, whereas ACE was positioned around 240 R_E. This separation increases the uncertainty in the calculation of correct propagation times. It should also be noted that the time lags represent the total delay for the large-scale convection to respond to changes at the assumed average magnetopause position of 11 R_E.

Using the average *ASY-H* magnetic index instead of Φ_{pc} in the correlation with the solar wind, results in the linear best fits displayed in Fig. 4c-d for the time lags of peak correlation. Performing a linear regression analysis for the *ASY-H* response to E_r at Δt=35 min gives the expression $y(x) = 15.8x + 10.8$. The third peak at Δt=80 min results in $y(x) = 11.9x + 15.4$. As the delay time increases, the best fit slope is observed to gradually decrease. This implies that on the average, the shorter the delay is, the larger the depression for a constant reconnection electric field at the magnetopause. An underlying assumption is that *ASY-H* at any one time reflects the superposition of contributions from direct input responses as well as delayed geomagnetic tail

responses.

In comparing Fig. 4b with Fig. 4d we note that there is a larger scatter for the Φ_{pc} data than for *ASY-H*, which may be attributed to the effect of not measuring the complete cross-polar potential drop. The solid line in Fig. 4c only uses the 73 points shown, while the dotted line also includes the four points with IMF $B_z > 3$ nT.

The two studies are clearly different for both the *ASY-H* response and the Φ_{pc} response. For the FAST study, with data from July 1997, the geomagnetic activity was lower than $Kp = 4^-$ and the major response of *ASY-H* to E_r peaked between 60 and 75 min. Here, with a maximum $Kp = 7^-$, we mainly observe a twin peak with an initial fast response at Δt=35 min and a second peak at 65 min time lag. This difference may be due to the effect of examining the magnetospheric response for different levels of geomagnetic activity. The largest potential drop included in this data set, Φ_{pc}=204 kV (see Fig. 1 for the electric field), was measured approximately 10 hours after the magnetic storm on 18 February had reached a minimum $Dst = -134$ nT. Moreover, this data set contains a total of 21 events when the geomagnetic activity level was greater than $Kp = 4^-$.

Bargatze et al. (1985) reported on two major pulses at about a 20 and 60 min time lag in their study of the westward electrojet AL index response to the solar wind input vB_s for different levels of geomagnetic activity. As the level of geomagnetic activity increased from moderate to strong, they discovered that the directly driven 20 min response started to dominate over the 60 min unloading response. Both pulses were present for moderate activities, but the 60 min response was more pronounced. In this study of higher geomagnetic activity, the Φ_{pc} response to E_r has a broad single peak around 25 min lag, whereas *ASY-H* responded to E_r with three multiple peaks of 35, 65, and 80 min lags. In an earlier study, using FAST data for a lower level of geomagnetic activity, a mirror image was found. The Φ_{pc} then responded to E_r with three multiple peaks, whereas *ASY-H* responded with one broad peak around a 60–75 min lag. We believe these differences may be attributed to different levels of geomagnetic activity and to differences in the overall geophysical conditions for the different events. This follows from studying the AL response to vB_s for different geomagnetic activities, as shown in Fig. 3 of Bargatze et al. (1985). By going from their filter 21 to filter 14 say (i.e. from higher activity to lower activity), we observe two peaks at approximately 20 min and 55 min in filter 21, but only one broad peak around 60 to 70 min of filter 14. This trend is observed for the *ASY-H* response to E_r going from the Astrid-2 results to the FAST results (Eriksson et al., 2000). A similar trend is observed for Φ_{pc} to E_r, going from filter 27 of higher activity, showing a single broad peak around 20 min, to filter 21 of lower activity.

The auroral electrojets have been reported to respond only on the shorter 20 min time scale for periods of enhanced geomagnetic activity (Baker et al., 1983). This may explain the lack of clear secondary unloading responses to the reconnection electric field for Φ_{pc}, which was observed, however, to

occur in the FAST study for a lower level of geomagnetic activity.

The *ASY-H* response to the reconnection electric field examined here is further quantitatively consistent with the results obtained by Clauer and McPherron (1980), in which they report that large low-latitude asymmetric disturbances (> 25 nT) were consistently preceeded by an enhanced dawn-dusk solar wind electric field for a total of 24 events.

To summarize, we have examined the average time delayed response of the ionospheric convection and the low-latitude horizontal geomagnetic disturbance to the 5-min resolution reconnection electric field for a total of 77 events. We find that it is possible to observe the directly driven response of the high-latitude convection around 25 min, and the delayed unloading response of the field-aligned current system primarily around 65 min, as measured by *ASY-H*. These individual responses were also identified by Eriksson et al. (2000) for a lower geomagnetic activity level. We further suggest that the high level of geomagnetic activity recorded in this study increases the efficiency for the solar wind to directly drive the region 1 and region 2 field-aligned current systems, which are believed to be a major cause for the low-latitude asymmetric depression in the horizontal component of the geomagnetic field (Crooker and Siscoe, 1981). This earlier *ASY-H* response is estimated to be delayed by 35 min after the solar wind has reached the magnetopause, which is somewhat longer than for the convection to respond. This may support the idea proposed by Clauer et al. (1983) that the reconnection electric field primarily drives the ionospheric convection and that the global Birkeland current system, in turn, must respond to changes in the convection. However, it is the purpose of a future study to verify the possible internal delays between the ionospheric convection and the westward electrojet, since in the study of Bargatze et al. (1985), only AL was used and Φ_{pc} was omitted.

References

Baker, D. N., Zwickl, R. D., Bame, S. J., Hones, E. W. Jr., Tsurutani, B. T., Smith, E. J., and Akasofu, S.-I., An ISEE 3 high time resolution study of interplanetary parameter correlations with magnetospheric activity, J. Geophys. Res., 88, 6230–6242, 1983.

Bargatze, L. F., Baker, D. N., McPherron, R. L., and Hones, E. W. Jr., Magnetospheric impulse response for many levels of geomagnetic activity, J. Geophys. Res., 90, 6387–6394, 1985.

Blanchard, G. T. and McPherron, R. L., Analysis of the linear response function relating AL to VB_s, J. Geophys. Res., 100, 19155–19165, 1995.

Clauer, C. R. and McPherron, R. L., The relative importance of the interplanetary electric field and magnetospheric substorms on partial ring current development, J. Geophys. Res., 85, 6747–6759, 1980.

Clauer, C. R., McPherron, R. L., and Searls, C., Solar wind control of the low-latitude asymmetric magnetic disturbance field, J. Geophys. Res., 88, 2123–2130, 1983.

Crooker, N. U. and Siscoe, G. L., Birkeland currents as the cause of the low-latitude asymmetric disturbance field, J. Geophys. Res., 86, 11201–11210, 1981.

Efron, B. and Tibshirani, R. J., An Introduction to the Bootstrap, Mono. Stat. Appl. Prob., 57, 436 pp., Chapman and Hall, New York, 1993.

Eriksson, S., Ergun, R. E., Carlson, C. W., and Peria, W., The cross-polar potential drop and its correlation to the solar wind, J. Geophys. Res., 105, 18639–18653, 2000.

Etemadi, A., Cowley, S. W. H., Lockwood, M., Bromage, B. J. I., Willis, D. M., and Luhr, H., The dependence of high-latitude ionospheric flows on the north-south component of the IMF: A high time resolution correlation analysis using EISCAT Polar and AMPTE UKS and IRM data, Planet. Space Sci., 36, 471–498, 1988.

Fairfield, D. H., Average and unusual locations of the Earth's magnetopause and bow shock, J. Geophys. Res., 76, 6700–6716, 1971.

Fukushima, N. and Kamide, Y., Partial ring current models for worldwide geomagnetic disturbances, Rev. Geophys. Space Phys., 11, 795–853, 1973.

Harel, M., Wolf, R. A., Reiff, P. H., Spiro, R. W., Burke, W. J., Rich, F. J., and Smiddy, M., Quantitative simulation of a magnetospheric substorm, 1, Model logic and overview, J. Geophys. Res., 86, 2217–2241, 1981.

Holzer, T. E. and Reid, G. C., The response of the dayside magnetosphere-ionosphere system to time-varying field line reconnection at the magnetopause, I, Theoretical model, J. Geophys. Res., 80, 2041–2049, 1975.

Iyemori, T., Maeda, H., and Kamei, T., Impulse response of geomagnetic indices to interplanetary magnetic field, J. Geomagn. Geoelectr., 31, 1–9, 1979.

Iyemori, T. and Rao, D. R. K., Decay of the *Dst* field of geomagnetic disturbance after substorm onset and its implication to storm-substorm relation, Ann. Geophysicae, 14, 608–618, 1996.

Lockwood, M., Cowley, S. W. H., and Freeman, M. P., The excitation of plasma convection in the high-latitude ionosphere, J. Geophys. Res., 95, 7961–7972, 1990.

Reiff, P. H. and Luhmann, J. G., Solar wind control of the polar-cap voltage, in: Solar Wind-Magnetosphere Coupling, Eds. Y. Kamide and J. A. Slavin, pp. 453–476, Terra Sci., Tokyo, 1986.

Sanchez, E. R., Siscoe, G. L., and Meng, C.-I., Inductive attenuation of the transpolar voltage, Geophys. Res. Lett., 18, 1173–1176, 1991.

Shue, J.-H. and Weimer, D. R., The relationship between ionospheric convection and magnetic activity, J. Geophys. Res., 99, 401–415, 1994.

Todd, H., Cowley, S. W. H., Etemadi, A., Bromage, B. J. I., Lockwood, M., Willis, D. M., and Luhr, H., Response-time of the high-latitude ionosphere to sudden changes in the north-south component of the IMF, Planet. Space Sci., 36, 1415–1428, 1988.

Weimer, D. R., A flexible, IMF-dependent model of high-latitude electric potentials having "space weather" applications, Geophys. Res. Lett., 23, 2549–2552, 1996.